Joule heating of the south polar terrain on Enceladus

K. P. Hand,[1] K. K. Khurana,[2] and C. F. Chyba[3]

Received 12 November 2010; revised 1 February 2011; accepted 13 February 2011; published 27 April 2011.

[1] We report that Joule heating in Enceladus, resulting from the interaction of Enceladus with Saturn's magnetic field, may account for 150 kW to 52 MW of power through Enceladus. Electric currents passing through subsurface channels of low salinity and just a few kilometers in depth could supply a source of power to the south polar terrain, providing a small but previously unaccounted for contribution to the observed heat flux and plume activity. Studies of the electrical heating of Jupiter's moon Europa have concluded that electricity is a negligible heating source since no connection between the conductive subsurface and Alfvén currents has been observed. Here we show that, contrary to results for the Jupiter system, electrical heating may be a source of internal energy for Enceladus, contributing to localized heating, production of water vapor, and the persistence of the "tiger stripes." This contribution is of order 0.001–0.25% of the total observed heat flux, and thus, Joule heating cannot explain the total south polar terrain heat anomaly. The exclusion of salt ions during refreezing serves to enhance volumetric Joule heating and could extend the lifetime of liquid water fractures in the south polar terrain.

Citation: Hand, K. P., K. K. Khurana, and C. F. Chyba (2011), Joule heating of the south polar terrain on Enceladus, *J. Geophys. Res.*, *116*, E04010, doi:10.1029/2010JE003776.

1. Introduction

[2] The relative motion of a moon, or secondary, through the magnetic field of its primary may result in a host of electromagnetic effects, depending on the internal composition and geological activity of the secondary [*Panofsky and Phillips*, 1962; *Sonett et al.*, 1970; *Kivelson et al.*, 2004]. In particular, unipolar induction may result from the Lorentz force $\mathbf{F} = q(\mathbf{v} \times \mathbf{B})$, where $\mathbf{v}$ is the relative velocity of the secondary, $\mathbf{B}$ is the field of the primary, and q is the charge quantum. Unipolar induction applied to planetary bodies was first explored by *Piddington and Drake* [1968] and *Goldreich and Lynden-Bell* [1969] for the case of Io. In this hypothesis, currents flow through the ionosphere of Jupiter, down the flux tube to the sub-Jovian equatorial region of Io, through Io, and then back to Jupiter after exiting at the anti-Jovian equatorial region. However, the dense plasma and mass loading from the ionosphere into the Io torus likely shunt this circuit yielding little Joule heating internal to Io [*Goertz*, 1980; *Saur et al.*, 2004].

[3] *Sonett et al.* [1970] explored unipolar induction for a variety of worlds, including asteroids, comets, and the Moon. *Colburn and Reynolds* [1985] considered Europa and found the resulting potential to be 82 kV per hemisphere. At Europa, however, the flow of current is impeded by a very insulating ice shell; only if the external flux tube current contacts the conducting ocean water through fractures in the ice will significant currents pass through the ocean and generate heat. Absent evidence for an active Europan ice shell that allows for such a circuit, little more can be said about currents passing through Europa.

[4] Recent observations by the Cassini spacecraft, however, present several compelling reasons to consider unipolar induction and Joule heating for Saturn's moon Enceladus. First, the observations of plume activity [*Dougherty et al.*, 2006; *Spencer et al.*, 2006; *Porco et al.*, 2006], plume chemistry [*Waite et al.*, 2009; *Postberg et al.*, 2009], and surface deformation [*Collins and Goodman*, 2007] make a strong case for a subsurface liquid water reservoir. Second, plume activity is concentrated along four parallel linear features ("tiger stripes") that dominate the south polar terrain (SPT); these features are ~150 km long and roughly evenly spaced at ~30 km intervals. The combination of active fractures in the surface ice and a possible subsurface conducting region provide the conditions needed for unipolar induction and Joule heating.

[5] In addition, the ionosphere of Saturn provides some clues to the magnetospheric connection with Enceladus. In the Jovian system the magnetic field interaction with the satellites Io, Europa, and Ganymede is clearly visible in the auroral footprint of Jupiter's ionosphere [*Clarke et al.*, 2002]. The Saturnian system, however, has a weaker magnetic field and the axis of the dipole component is aligned with the rotation axis of Saturn; consequently emissions resulting from the interaction of the saturnian magnetosphere with the

[1]Jet Propulsion Laboratory, California Institute of Technology, Pasadena, California, USA.
[2]Department of Planetary Sciences, University of California, Los Angeles, California, USA.
[3]Department of Astrophysical Sciences, Princeton University, Princeton, New Jersey, USA.

0148-0227/11/2010JE003776

plume environment of Enceladus are expected to be just a few tenths of a kilorayleigh. Consistent with the detection limits of the Hubble Space Telescope, no such emissions were identified [*Wannawichian et al.*, 2008]. Recent Cassini observations, however, show an auroral spot on Saturn associated with Enceladus. This auroral activity indicates the flow of currents in the region around or within Enceladus [*Rymer et al.*, 2009, 2010; *Pryor et al.*, 2009].

[6] Finally, Joule heating is important to consider because the anomalously large heat flux of more than 5.8 GW, and possible more than 15 GW [*Spencer et al.*, 2010], measured for the SPT is considered by some to be a "puzzle" [*Meyer and Wisdom*, 2007]. While tidal heating may be a sufficient explanation [*Ross and Schubert*, 1989] other sources of heating are important to consider.

2. Model

[7] Saturn's magnetic field and rotation axes are nearly aligned. The vertical component of the magnetic field at Enceladus is 325 nT and the relative motion of the plasma in the frame of the moon is 26.1 km s^{-1} [*Dougherty et al.*, 2006]. Due to slowing of the plasma in the region around Enceladus, the relative velocity of the plasma parcels that encounter Enceladus may be less than 26.1 km s^{-1} [*Neubauer*, 1980; *Khurana et al.*, 2007; *Tokar et al.*, 2009]. The resulting electric field, $E = -vB$, has a maximum value of -8.5×10^{-3} V m^{-1}, leading to a change in potential of ~4300 V across the full diameter of Enceladus or ~1100 V across the SPT.

[8] The electric field clearly scales with any reduction in relative velocity. During the initial formation of the tiger stripes features, and prior to the formation of the large plume, the relative velocity, and thus the electric field, would have been at a maximum because there would have been no conductive disturbance around Enceladus. Any reduction in relative velocity lowers the potential across the SPT. Interestingly however, a reduction in velocity leads to an increase in the plasma density in the region of the SPT and likely leads to an increase in current available to the SPT. As shown below, the current scales with the square root of the plasma density and thus the increased current compensates for the reduction in potential.

[9] The current available through an Alfvén wing is the integral of the surface current density,

$$j = 2\frac{B}{\mu_0}\left(1 - \frac{E_i}{E_0}\right)\sin\phi\sin\theta, \tag{1}$$

over the surface area of the cross-section closure supplied by the conducting region [*Neubauer*, 1980]. Here E_0 is the electric field external to the Alfvén wing and E_i is the field internal to the conducting region. The angles ϕ and θ are the Alfvén wing cross-section angle over which to integrate the current density and the Alfvén wing bend angle, respectively. As shown by *Neubauer* [1980], the bend angle is related to the Alfvén conductance, Σ_A, by

$$\sin\theta = \frac{\mu_0\Sigma_A E_0}{B}. \tag{2}$$

The Alfvén conductance is $\sim 1/\mu_0 V_A$ where the Alfvén velocity is $V_A = B/\sqrt{\mu_0\rho}$ and ρ is the plasma density, which for the case of Enceladus is based on Cassini measurements [*Khurana et al.*, 2007; *Persoon et al.*, 2009]. Integration of ϕ is typically done over 0 to π to account for current flowing in and out of the full disk, but in our analyses we also consider the case in which only a fraction of the current available in the disk flows through a conductive path made accessible by the tiger stripes.

[10] For a moon the integrated current supplied by the Alfvén wing over the full cross section yields a total current, $I = 4(E_0 - E_i)R\Sigma_A$. The radius R denotes the radius of the Alfvén wing column and is typically equal to, or greater than, the radius of the object obstructing the plasma (i.e., $R \sim R_{\text{Enceladus}}$).

3. Results

[11] The available current and electrical potential lead to power dissipation within a conducting region of Enceladus given by [*Neubauer*, 1980]

$$P = 4\pi R^2\Sigma_A E_i(E_0 - E_i). \tag{3}$$

Maximum Joule heating occurs for impedance matching of the internal and external loads, such that $E_i = E_0/2$ and, $P_{\max} = \pi R^2\Sigma_A E_0^2$. If Enceladus harbors a global subsurface ocean and fractures on the sub-Saturnian and anti-Saturnian faces permit connection of the ocean to the plasma, then the full radius of the moon could yield $P_{\max} = 52$ MW. For the specific case of the SPT, where the observed plumes provide direct evidence of communication with the subsurface, the appropriate R is defined by the length, L, of the tiger stripes. Observations show $L \sim 150$ km [*Porco et al.*, 2006] with a strike of approximately 30° off the radial line from Saturn, leading to an effective length of ~130 km and $R \sim 65$ km. Figure 1 shows the magnetic field and electric current configuration for the SPT. For the case of a south polar sea of radius ~65 km and with sufficient surface connection to harness the full integrated current of the Alfvén disk, maximum power dissipation due to Joule heating is 3.5 MW. Considering just one tiger stripe with a spatial extent capable of only harnessing a 45° swath of the full disk of current density at the sub- and anti-Saturnian regions, $P_{\max} = 2.7$ MW. Similarly, a reduction in relative velocity by 20% or 40% due to slowing of the plasma in the region of Enceladus leads to a reduced potential and maximum power dissipation of 2.2 and 1.3 MW, respectively.

[12] If, as mentioned above and by *Farrell et al.* [2009], the reduction in relative velocity leads to a denser plasma in the region around the SPT then the increased capacity for sourcing current to the SPT could maintain $P_{\max}$ at ~3.5 MW, as increased current compensates for loss in potential. Increasing the plasma density from 60 particles per cm^3 to roughly 600 particles per cm^3 leads to a threefold increase in $P_{\max}$.

[13] However, observations of electron dropout near Enceladus [*Farrell et al.*, 2009] raise interesting questions about the mobility of charge through the plumes and into Enceladus' interior. Measurements from the Cassini Radio and Plasma Wave System (RPWS) indicate a possible decrease in electron density from ~90 el cm^{-3} to below 20 el cm^{-3} and a decrease in velocity to 7 km s^{-2} during closest encounter. The cause of the dropout is not entirely clear, but if the electrons are being absorbed by ice grains and not

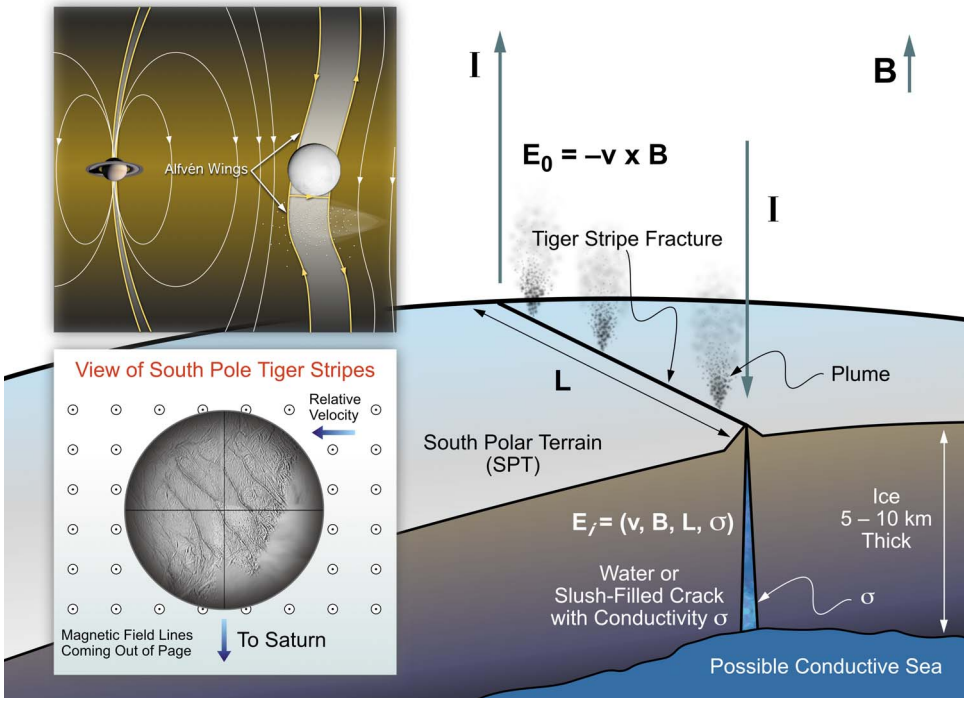

Figure 1. Schematic diagram of electromagnetic interactions along conducting fractures of the south polar terrain of Enceladus. The inset shows the global-scale magnetic field flow past Enceladus and the field disturbance observed by the Cassini spacecraft [*Khurana et al.*, 2007]. If the tiger stripe fractures permit connection of the magnetospheric plasma to a conducting liquid or slush within the fractures, then currents will flow and Joule heating will occur. The magnitude of heating depends on the magnetic field strength, the relative velocity of the plasma, the length and volume of the fracture, and the conductivity of the material.

available for current flow then the low-end estimates for power available for Joule heating across Enceladus' diameter and across the tiger stripes drops to 2.2 and 0.15 MW, respectively.

[14] The above calculations lead to a range of 150 kW to 52 MW for P_{max}, with the SPT geometrically constrained value being ~3.5 MW for a charge density of 60 particles per cm^3 and a relative velocity of 26.1 km s^{-1}.

[15] Impedance matching, and hence power dissipation, depends on the conductivity of the ice or water in the subsurface. Considering power per unit volume, σE_i^2, we calculate power dissipation as a function of conductivity and hence salt concentration. For a given volume, V, we solve for the conductivity of the water, σ, via

$$\sigma = \frac{4\pi\Sigma_A L^2 \cos^2\phi(E_0 - E_i)}{VE_i} \quad (4)$$

and find power dissipation as a function of subsurface conductivity, $P = \sigma E_i^2 V$.

[16] To examine power dissipation as a function of salinity we consider a subsurface sea of volume $L^2 d$, where d is the depth of the sea, and cases in which conductive fractures of length L and cross-sectional area A supply the current path. Figure 2 shows results for Joule heating in the south polar terrain of Enceladus as a function of conductivity, relative velocity, and conductor volume. The maximum power is constant, 3.5 MW, but as conductivity, and hence salinity, increases smaller volumes are required to achieve maximum power dissipation. Volumes chosen represent test cases for tiger stripe and SPT geometry and are as follows: (1) a conductive subsurface south polar sea with dimensions 150 × 150 km by 10 km deep; (2) a single tiger stripe with a subsurface conducting region 1 km wide by 150 km long and 10 km deep; and (3) a single tiger stripe with a subsurface conducting region 100 m wide by 150 km long by 5 km deep. The dimensions for cases 2 and 3 were selected to be consistent with the geometry of the tiger stripes and geophysical models for Enceladus [*Porco et al.*, 2006; *Nimmo et al.*, 2007; *Barr and McKinnon*, 2007]. They were also chosen to achieve near-maximum power dissipation for a conductivity corresponding to that of low-end estimates for the salinity of water in Enceladus [*Zolotov*, 2007; *Postberg et al.*, 2009; *Schneider et al.*, 2009] (case 2) and that of the Earth's ocean, with σ = 2.75 S m^{-1} (case 3). Results for cases 2 and 3 are also applicable to the configuration of four fractures at one quarter of the above defined widths, e.g., case 2 can correspond to four fractures 250 m wide and case 3 can correspond to four fractures 25 m wide. Interestingly, volumes considerably smaller than case 3 require conductivities that are too high to be achieved with salt water solutions [*Hand and Chyba*, 2007]. Larger volumes (e.g., a south polar sea as in case 1) achieve maximum Joule heating when conductivities are considerably less than terrestrial ocean conductivity; values

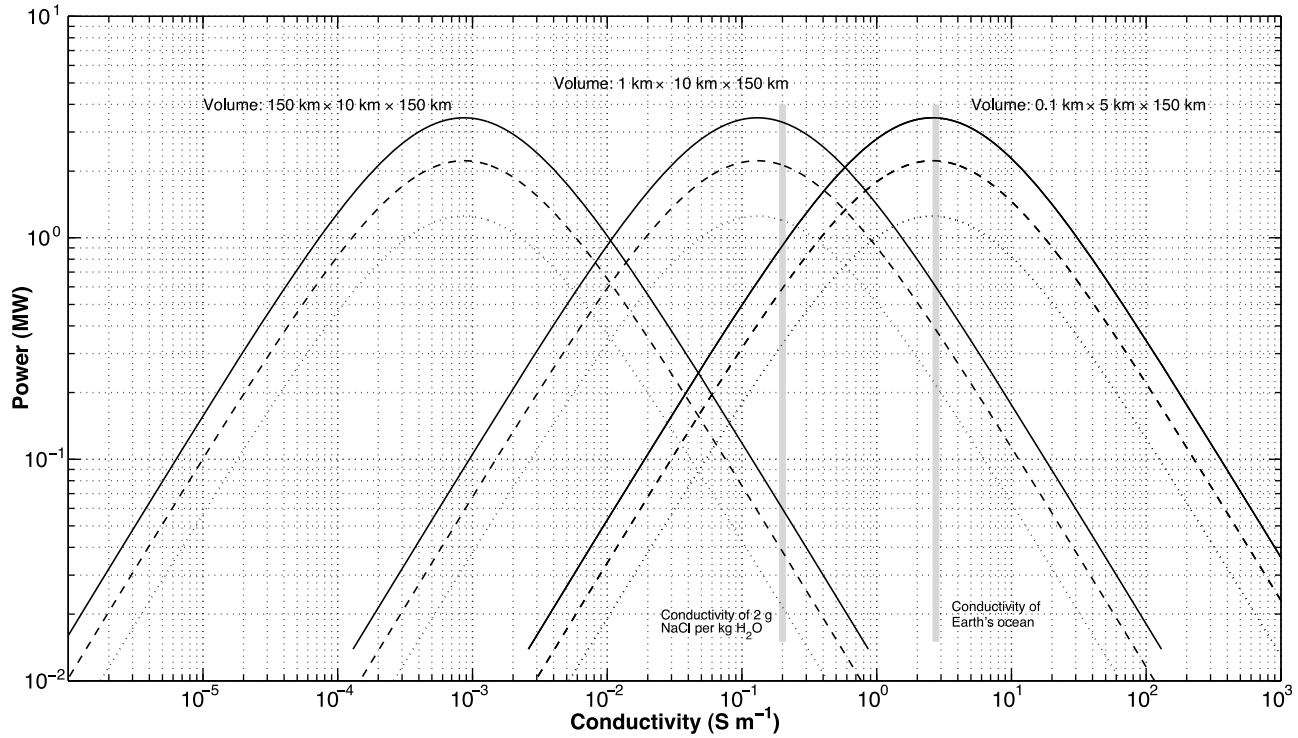

Figure 2. Total power from Joule heating in the south polar terrain of Enceladus as a function of conductivity, relative velocity, and conductor volume. Cases 1, 2, and 3 as described in the text are shown from left to right. Solid lines indicate a relative velocity of 26 km s^{-1} (100% of Enceladus' relative velocity), dashed lines indicate 20.8 km s^{-1} (80% of Enceladus' relative velocity), dotted lines indicate 15.6 km s^{-1} (60% of Enceladus' relative velocity). For a given volume of subsurface conductive material (salt water), there exists a conductivity for which power dissipation achieves a maximum. Conductivities corresponding to Earth's ocean (2.75 S m^{-1}) and low-end estimates for Enceladus [*Postberg et al.*, 2009; *Zolotov*, 2007; *Schneider et al.*, 2009] are shown.

of 10^{-3}–10^{-4} S m^{-1} are comparable to normal "tap" water for drinking.

4. Discussion

[17] The few tenths to tens of megawatts of power available from Joule heating in the SPT cannot explain the several gigawatts of power radiating from the surface [*Spencer et al.*, 2006]; however, Joule heating does provide a mechanism through which energy in the magnetosphere of Saturn can be transferred to the SPT of Enceladus. Though tidal heating and shear heating have been invoked to explain the surface heat flux [*Meyer and Wisdom*, 2007; *Nimmo et al.*, 2007], both mechanisms suffer limitations. Tidal heating cannot explain the initiation of the heat flux; a low-viscosity or liquid water region is required ab initio to permit significant tidal heating. Shear heating is proposed to produce at most 285 MW per 150 km [*Nimmo et al.*, 2007]. Decomposition of clathrates has also been invoked [*Kieffer et al.*, 2006]. Common among many of these models is an assumed preexisting heat source capable of producing liquid water coupled to the proposal that latent heat from liquid water or sublimation can explain the thermal signature of the SPT. Joule heating also suffers from the initialization problem; without a salty liquid water conducting region in contact with the surface no currents will flow [*Reynolds et al.*, 1983].

[18] As reported by *Nimmo et al.* [2007] and *Tian et al.* [2007], the recondensation of ~10^3 kg s^{-1} of water vapor could yield much of the observed 3–7 GW of power. Based on the calculation presented here, we conclude that Joule heating could provide a small source for generating water vapor that recondenses on the surface. Joule heating of 0.15–50 MW could contribute 0.15–50 kg s^{-1} of vapor to the plume, amounting to a few percent of the vapor flux [*Tian et al.*, 2007].

[19] An interesting geophysical consequence of Joule heating is that it may serve to prevent, or at least abate, freezing and sealing of existing fractures. The conductivity corresponding to $P_{\max}$ is

$$\sigma = \frac{16}{\pi^2 d}\Sigma_A \sim \frac{\Sigma_A}{d}. \tag{5}$$

[20] In other words, for a given Alfvén conductance the conductivity of the sea corresponding to maximum Joule heating is inversely proportional to the depth of the sea. Deeper seas require lower conductivity, i.e., lower salt concentrations, to achieve $P_{\max}$. Herein lies an interesting relationship: as freezing occurs conductivity increases due to ion exclusion and the remaining conductive solution may maintain maximum dissipation. Once a fracture opens, refreezing will serve to concentrate solutes and ions, thus

increasing conductivity while decreasing volume. The total Joule heating will not change because **v**, **B**, and L remain constant, but the volumetric heating increases and serves to impede further freezing.

[21] Future Cassini flybys of Enceladus will help further constrain the solute concentration of both the surface ice and plume material, thereby allowing an improved understanding of possible Joule heating in the subsurface. Magnetic field perturbations resulting from any currents running through the SPT are unlikely to be detected. Using an idealized case where $B = \mu_0 I/2\pi r$ and a maximum current of ~4000 A, we calculate an effect on the order of a few nanotesla for a closest approach, r, of 100 to 50 km.

[22] **Acknowledgments.** K. P. Hand acknowledges support from the Jet Propulsion Laboratory, California Institute of Technology, through a contract with NASA, and support through the NASA Astrobiology Institute, Astrobiology of Icy Worlds' team at the Jet Propulsion Laboratory.

References

Barr, A., and W. McKinnon (2007), Convection in Enceladus' ice shell: Conditions for initiation, *Geophys. Res. Lett.*, *34*, L09202, doi:10.1029/2006GL028799.

Clarke, J., et al. (2002), Ultraviolet emissions from the magnetic footprints of Io, Ganymede and Europa on Jupiter, *Nature*, *415*(6875), 997–1000, doi:10.1038/415997a.

Colburn, D., and R. Reynolds (1985), Electrolytic currents in Europa, *Icarus*, *63*(1), 39–44, doi:10.1016/0019-1035(85)90019-3.

Collins, G., and J. Goodman (2007), Enceladus' south polar sea, *Icarus*, *189*(1), 72–82, doi:10.1016/j.icarus.2007.01.010.

Dougherty, M., K. Khurana, F. Neubauer, C. Russell, J. Saur, J. Leisner, and M. Burton (2006), Identification of a dynamic atmosphere at Enceladus with the Cassini magnetometer, *Science*, *311*(5766), 1406–1409, doi:10.1126/science.1120985.

Farrell, W. M., W. S. Kurth, D. A. Gurnett, R. E. Johnson, M. L. Kaiser, J.-E. Wahlund, and J. H. Waite Jr. (2009), Electron density dropout near Enceladus in the context of water-vapor and water-ice, *Geophys. Res. Lett.*, *36*, L10203, doi:10.1029/2008GL037108.

Goertz, C. (1980), Io's interaction with the plasma torus, *J. Geophys. Res.*, *85*(A6), 2949–2956, doi:10.1029/JA085iA06p02949.

Goldreich, P., and D. Lynden-Bell (1969), Io, a Jovian unipolar inductor, *Astrophys. J.*, *156*, 59–78, doi:10.1086/149947.

Hand, K., and C. Chyba (2007), Empirical constraints on the salinity of the Europan ocean and implications for a thin ice shell, *Icarus*, *189*(2), 424–438, doi:10.1016/j.icarus.2007.02.002.

Khurana, K., M. Dougherty, C. Russell, and J. Leisner (2007), Mass loading of Saturn's magnetosphere near Enceladus, *J. Geophys. Res.*, *112*, A08203, doi:10.1029/2006JA012110.

Kieffer, S., X. Lu, C. Bethke, J. Spencer, S. Marshak, and A. Navrotsky (2006), A clathrate reservoir hypothesis for Enceladus' south polar plume, *Science*, *314*(5806), 1764–1766, doi:10.1126/science.1133519.

Kivelson, M., F. Bagenal, W. Kurth, F. Neubauer, C. Paranicas, and J. Saur (2004), Magnetospheric interactions with satellites, in *Jupiter: The Planet, Satellites and Magnetosphere*, pp. 513–536, Cambirdge Univ. Press, Cambridge, U. K.

Meyer, J., and J. Wisdom (2007), Tidal heating in Enceladus, *Icarus*, *188*(2), 535–539, doi:10.1016/j.icarus.2007.03.001.

Neubauer, F. (1980), Nonlinear standing Alfvén wave current system at Io: Theory, *J. Geophys. Res.*, *85*(A3), 1171–1178, doi:10.1029/JA085iA03p01171.

Nimmo, F., J. Spencer, R. Pappalardo, and M. Mullen (2007), Shear heating as the origin of the plumes and heat flux on Enceladus, *Nature*, *447*(7142), 289–291, doi:10.1038/nature05783.

Panofsky, W. K. H., and M. Phillips (1962), *Classical Electricity and Magnetism*, Addision-Wesley, Reading, Mass.

Persoon, A. M., et al. (2009), A diffusive equilibrium model for the plasma density in Saturn's magnetosphere, *J. Geophys. Res.*, *114*, A04211, doi:10.1029/2008JA013912.

Piddington, J., and F. Drake (1968), Electrodynamic effects of Jupiter's satellite Io, *Nature*, *217*, 935–937, doi:10.1038/217935a0.

Porco, C., et al. (2006), Cassini observes the active south pole of Enceladus, *Science*, *311*(5766), 1393–1401, doi:10.1126/science.1123013.

Postberg, F., S. Kempf, J. Schmidt, N. Brilliantov, A. Beinsen, B. Abel, U. Buck, and R. Srama (2009), Sodium salts in E-ring ice grains from an ocean below the surface of Enceladus, *Nature*, *459*(7250), 1098–1101, doi:10.1038/nature08046.

Pryor, W., et al. (2009), Saturn auroral movies from Cassini UVIS, *Eos Trans. AGU*, *90*(52), Fall Meet. Suppl., Abstract SM32B-01.

Reynolds, R., S. Squyres, D. Colburn, and C. McKay (1983), On the habitability of Europa, *Icarus*, *56*, 246–254, doi:10.1016/0019-1035(83)90037-4.

Ross, M., and G. Schubert (1989), Viscoelastic models of tidal heating in Enceladus, *Icarus*, *78*(1), 90–101, doi:10.1016/0019-1035(89)90071-7.

Rymer, A., D. Mitchell, H. Smith, A. Coates, and M. Dougherty (2009), Evidence for Enceladus link to Saturn ionosphere: Does the plume have an auroral footprint?, paper presented at 41st Annual Meeting of the Division for Planetary Sciences, Am. Astron.Soc., Fajardo, Puerto Rico.

Rymer, A., et al. (2010), Discovery of the Enceladus auroral footprint and evidence for an extended plasma torus, paper presented at 42nd Annual Meeting of the Division for Planetary Sciences, Am. Astron. Soc., Pasadena, Calif.

Saur, J., F. Neubauer, J. Connerney, P. Zarka, and M. Kivelson (2004), Plasma interaction of Io with its plasma torus, in *Jupiter: The Planet, Satellites and Magnetosphere*, pp. 537–560, Cambirdge University Press, Cambridge, U. K.

Schneider, N., M. Burger, E. Schaller, M. Brown, R. Johnson, J. Kargel, M. Dougherty, and N. Achilleos (2009), No sodium in the vapour plumes of Enceladus, *Nature*, *459*(7250), 1102–1104, doi:10.1038/nature08070.

Sonett, C., D. Colburn, K. Schwartz, and K. Keil (1970), The melting of asteroidal-sized bodies by unipolar dynamo induction from a primordial T Tauri sun, *Astrophys. Space Sci.*, *7*(3), 446–488, doi:10.1007/BF00653283.

Spencer, J., J. Pearl, M. Segura, F. Flasar, A. Mamoutkine, P. Romani, B. Buratti, A. Hendrix, L. Spilker, and R. Lopes (2006), Cassini encounters Enceladus: Background and the dDiscovery of a south polar hot spot, *Science*, *311*(5766), 1401–1405, doi:10.1126/science.1121661.

Spencer, J., C. Howett, J. Pearl, A. Verbiscer, T. Hurford, and M. Segura (2010), Endogenic thermal emission from Enceladus' south pole observed by the Cassini Composite Infrared Spectrometer, paper presented at EGU General Assembly, Vienna, Austria.

Tian, F., A. Stewart, O. Toon, K. Larsen, and L. Esposito (2007), Monte Carlo simulations of the water vapor plumes on Enceladus, *Icarus*, *188*(1), 154–161, doi:10.1016/j.icarus.2006.11.010.

Tokar, R., R. Johnson, M. Thomsen, R. Wilson, D. Young, F. Crary, A. Coates, G. Jones, and C. Paty (2009), Cassini detection of Enceladus' cold water-group plume ionosphere, *Geophys. Res. Lett.*, *36*, L13203, doi:10.1029/2009GL038923.

Waite, J., et al. (2009), Liquid water on Enceladus from observations of ammonia and ^{4}0Ar in the plume, *Nature*, *460*(7254), 487–490, doi:10.1038/nature08153.

Wannawichian, S., J. Clarke, and D. Pontius Jr. (2008), Interaction evidence between Enceladus' atmosphere and Saturn's magnetosphere, *J. Geophys. Res.*, *113*, A07217, doi:10.1029/2007JA012899.

Zolotov, M. (2007), An oceanic composition on early and today's Enceladus, *Geophys. Res. Lett.*, *34*, L23203, doi:10.1029/2007GL031234.

C. F. Chyba, Department of Astrophysical Sciences, Princeton University, 4 Ivy Ln., Peyton Hall, Princeton, NJ 08544, USA.

K. P. Hand, Jet Propulsion Laboratory, California Institute of Technology, MS 183-601, 4800 Oak Grove Dr., Pasadena, CA 91109, USA. (Kevin.P.Hand@jpl.nasa.gov)

K. K. Khurana, Department of Planetary Sciences, University of California, 6863 Slichter Hall, Los Angeles, CA 90095-1567, USA.